TẠP CHÍ KHOA HỌC
TRƯỜNG ĐẠI HỌC QUY NHƠN

Thiết kế bộ quan sát $\mathcal{H}_\infty$ theo phương pháp chia lưới cho hệ Lorenz 63 sử dụng mô hình dạng phi tuyến với tham số thay đổi

Tác giả thứ 1[1,*], Tác giả thứ 2[1], Tác giả thứ 3[2,*]
[1]*Trường*
[2]*Trường*

Ngày nhận bài: .../.../2025; Ngày sửa bài: .../.../2025;
Ngày nhận đăng: .../.../2025; Ngày xuất bản: .../.../2025

TÓM TẮT

Bài báo này đề xuất một phương pháp thiết kế bộ quan sát $\mathcal{H}_\infty$ bền vững cho hệ Lorenz 63 thông qua mô hình hóa lại theo dạng hệ phi tuyến với tham số thay đổi (NLPV). Bằng cách sử dụng phương pháp chia lưới theo không gian trạng thái và xây dựng các mô hình tuyến tính cục bộ, chúng tôi thiết lập một tập hợp các bất đẳng thức ma trận tuyến tính (LMI) để thiết kế bộ quan sát tại mỗi điểm lưới. Các ma trận bộ quan sát thu được sẽ được nội suy theo thời gian thực dựa trên trạng thái của bộ quan sát. Phương pháp này cho phép ước lượng chính xác các trạng thái của hệ trong cả hai trường hợp có nhiễu và không nhiễu. Kết quả mô phỏng và so sánh với bộ lọc Kalman mở rộng (EKF) xác nhận hiệu quả của phương pháp đề xuất thông qua các chỉ số đánh giá Sai số bình phương trung bình (RMSE), Chuẩn hóa RMSE (NRMSE) và hệ số xác định R^2.

Từ khóa: *Hệ thống Lorenz, Bộ quan sát $\mathcal{H}_\infty$, Hệ phi tuyến với tham số thay đổi (NLPV), Tiếp cận LMI, Phương pháp chia lưới*

**Tác giả liên hệ chính.*
Email:<>

https://doi.org/10.52111/qnjs.2025.xxxxx

QUY NHON UNIVERSITY
JOURNAL OF SCIENCE

Gridding-Based $\mathcal{H}_\infty$ Observer Design for the Lorenz 63 System Using an NLPV Reformulation

[1st author, 2nd author, 3rd author]

[1]*University of ,*
[2]*University of ,*

Received: xx/xx/2025; Revised: xx/xx/2025;
Accepted: xx/xx/2025; Published: xx/xx/2025

ABSTRACT

This paper presents a robust $\mathcal{H}_\infty$ observer design for the Lorenz 63 system based on a Nonlinear Parameter-Varying (NLPV) reformulation. The nonlinear dynamics are approximated by gridding the state space and constructing local linear models. At each grid point, an observer gain is synthesized by solving a linear matrix inequality (LMI), with a common Lyapunov function ensuring stability across the operating range. The observer gain is updated online through barycentric interpolation based on the current estimated state. The approach enables real-time state estimation with guaranteed stability and disturbance attenuation. Simulation results under both noisy and noise-free conditions and comparison with an Extended Kalman Filter (EKF) confirm the effectiveness of the proposed design. Quantitative evaluations using Root Mean Square Error (RMSE), Normalized RMSE (NRMSE), and the coefficient of determination R^2 demonstrate high estimation accuracy and robustness of the observer across a range of dynamic behaviors in the Lorenz 63 system.

Keywords: *Lorenz system, $\mathcal{H}_\infty$ observer, Nonlinear parameter-varying (NLPV), LMI approach, Gridding method.*

1. INTRODUCTION

The Lorenz 63 system is a classical benchmark in nonlinear dynamics and chaos theory.[1-3] Due to its strong nonlinearities and sensitivity to initial conditions, it provides an ideal platform for testing observer design techniques. Designing observers for such systems is challenging, especially when dealing with unknown inputs, external disturbances, and nonlinearities.[4-8]

Traditional methods like the EKF often rely on linearization and statistical assumptions, which may not provide robustness in chaotic regimes.[9-10]

An alternative is the $\mathcal{H}_\infty$ observer framework, which focuses on worst-case disturbance attenuation.[11-13] However, applying $\mathcal{H}_\infty$ methods directly to nonlinear systems is difficult due to non-convexity.

To overcome this issue, the nonlinear system can be reformulated into an NLPV structure. The state space is discretized through gridding, and LMIs are employed to design observer gains at multiple linearization points. During online execution, the observer gain is interpolated in real-time based on the current estimated state using barycentric weights.[14] Although some existing works formulate the Lorenz system within a stochastic[15] framework using SDEs[9] and Itô calculus[16], this paper considers a purely deterministic ODE model and focuses on robust observer design without relying on statistical assumptions. Estimation performance is evaluated under both noisy and noise-free scenarios using standard quantitative metrics, including RMSE, NRMSE, and R^2. Results confirm the robustness and effectiveness of the observer design across a wide range of operating conditions.

**Corresponding author.*
Email:
https://doi.org/10.52111/qnjs.2025.xxxxx

The main contributions of this paper are summarized as follows:

- Provide a rigorous deterministic NLPV reformulation for the Lorenz-63 dynamics (starting from ODE) and clarify noise modeling assumptions (process and measurement).
- A grid-based $\mathcal{H}_\infty$ observer synthesis procedure using LMIs and a common Lyapunov function.
- A real-time gain scheduling strategy using barycentric interpolation based on the observer state.
- Simulation-based performance evaluation under noisy and noise-free conditions using RMSE, NRMSE, and R^2 metrics.

The rest of this paper is organized as follows. Section II presents the NLPV modeling of the Lorenz system. Section III introduces the observer design approach via gridding and LMIs. Section IV provides numerical simulations and evaluation. Section V concludes the paper.

2. SYSTEM MODELING AND NLPV REFORMULATION

This section presents a deterministic representation of the Lorenz–63 system and its reformulation into an NLPV structure suitable for LMI-based observer design. All noises in this paper are treated as exogenous additive disturbances, not intrinsic stochastic diffusions. Therefore, the Lorenz model is described by an ODE, consistent with its original formulation in Lorenz (1963).

2.1. Deterministic ODE form of the Lorenz System

The classical Lorenz–63 system is described by the nonlinear ordinary differential equation:

$$\dot{x}(t) = f(x(t)), x(t) \in \mathbb{R}^3, \quad (1)$$

where the nonlinear vector field is given by

$$f(x) = \begin{bmatrix} \sigma(x_2 - x_1) \\ x_1(\rho - x_3) - x_2 \\ x_1 x_2 - \beta x_3 \end{bmatrix}, \quad (2)$$

Here, x denotes the system state, and the classical Lorenz parameters are $\sigma = 10$, $\rho = 28$, and $\beta = \frac{8}{3}$.

To account for modeling uncertainties and external perturbations in a deterministic framework, the system is augmented with an additive process disturbance:

$$\dot{x}(t) = f(x(t)) + B_w w(t), \quad (3)$$

$$y(t) = Cx(t) + D_v v(t),$$

where $w(t)$, $v(t)$ denote process and measurement disturbances, respectively. These signals are treated as bounded-energy exogenous inputs, consistent with the $\mathcal{H}_\infty$ estimation framework. Equation (3) serves as the starting point for building an NLPV representation of the nonlinear dynamics.

2.2. Linearization and Jacobian-Based Approximation

To reformulate the nonlinear ODE into an NLPV structure, we use the Jacobian of $f(x)$:

$$J(x) = \frac{\partial f}{\partial x}(x) = \begin{bmatrix} -\sigma & \sigma & 0 \\ \rho - x_3 & -1 & -x_1 \\ x_2 & x_1 & -\beta \end{bmatrix} \quad (4)$$

Given that the Lorenz system evolves within a bounded region $\mathcal{D} \subset \mathbb{R}^3$, we approximate the nonlinear function locally by:

$$f(x) = J(x^{[i]})x + f_{\text{rem}}^{[i]}(x), \quad (5)$$

with, $x^{[i]}$ is a selected grid point, $f_{\text{rem}}^{[i]}(x) = f(x) - J(x^{[i]})x$ is the remainder term.

2.3. Lipschitz Property of the Nonlinear Remainder

For each grid region $\Omega_i \subset \mathcal{D}$, the remainder satisfies the following Lipschitz inequality:

$$\| f_{\text{rem}}^{[i]}(x_1) - f_{\text{rem}}^{[i]}(x_2) \| \leq L_f \| x_1 - x_2 \|, \quad (6)$$

$$\forall x_1, x_2 \in \Omega_i$$

A conservative global bound L_f can be computed as:

$$L_f = \sup_{x \in \mathcal{D}} \| J(x) \|_2, \quad (7)$$

where $\|\cdot\|_2$ is the spectral norm. The Lipschitz bound provides a structured way to handle the nonlinear remainder in the Lyapunov-based stability analysis without introducing stochastic assumptions.

2.4 NLPV Representation via Gridding

Let $\{x^{[1]}, \dots, x^{[N]}\}$ be the chosen grid points in $\mathcal{D}$. At each grid point, define:

$$A_i = J(x^{[i]}). \tag{8}$$

Using barycentric interpolation, the state-dependent linearization is:

$$A(\rho(t)) = \sum_{i=1}^{N} \mu_i(\rho(t)) A_i, \tag{9}$$

with barycentric weights:

$$\mu_i(\rho(t)) \geq 0, \sum_{i=1}^{N} \mu_i(\rho(t)) = 1. \tag{10}$$

where $\mu_i(\rho(t))$ are interpolation weights depending on the scheduling parameter $\rho(t)$.

The scheduling parameter is selected as:

$$\rho(t) = \hat{x}(t), \tag{11}$$

which ensures that all parameter-dependent quantities are available in real time without requiring access to the true state.

Combining the above results, the NLPV representation of the Lorenz–63 system is obtained as:

$$\begin{aligned} \dot{x}(t) &= A(\rho(t))\, x(t) + B_w w(t) + f_{\text{rem}}(x(t)) \\ y(t) &= Cx(t) + D_v v(t). \end{aligned} \tag{12}$$

where the nonlinear remainder $f_{\text{rem}}(x(t))$, satisfies the Lipschitz bound (6).

This formulation is now suitable for constructing an $\mathcal{H}_\infty$ observer via LMIs in Section 3.

Remark 1

The NLPV representation (11)–(12) is fully consistent with the original deterministic ODE (1)–(2) and does not introduce any stochastic interpretation or approximation of the system dynamics.

The gridding-based NLPV formulation admits a convex interpolation structure, which enables tractable LMI-based observer synthesis.

Retaining the nonlinear remainder explicitly avoids over-linearization and enables rigorous robustness analysis within the $\mathcal{H}_\infty$ framework.

3. OBSERVER DESIGN VIA GRIDDING

This section develops a robust state observer for the NLPV representation of the Lorenz–63 system introduced in Section 2. The proposed method relies on (i) formulating the estimation error dynamics, (ii) constructing an $\mathcal{H}_\infty$-type dissipation inequality to attenuate disturbances and nonlinear uncertainties, and (iii) enforcing stability across all grid points through convex LMIs using a common Lyapunov matrix.

3.1. NLPV System with Nonlinearity and Disturbance

The NLPV model obtained in Section 2 is rewritten in compact form as:

$$\begin{aligned} \dot{x}(t) &= A(\rho(t))x(t) + B_w w(t) + f_{\text{rem}}(x(t)) \\ y(t) &= Cx(t) + D_v v(t) \end{aligned} \tag{13}$$

where $x(t) \in \mathbb{R}^n$ is the system state, $w(t) \in \mathbb{R}^{n_w}$ is the process noise, $v(t) \in \mathbb{R}^{n_v}$ is the measurement disturbances. The matrices $A(\rho)$ and B_w are obtained by barycentric interpolation of the Jacobians and disturbance matrices at the selected grid points. The matrix D_v models a scheduling-dependent measurement noise channel. The nonlinear remainder $f_{\text{rem}}(x)$ is globally Lipschitz on the compact domain and satisfies:

$$\begin{aligned} &\| f_{\text{rem}}(x_1) - f_{\text{rem}}(x_2) \| \leq L_f \| x_1 - x_2 \|, \\ &\forall x_1, x_2 \in \mathcal{D},\ \mathcal{D} \subset \mathbb{R}^n \end{aligned} \tag{14}$$

This form isolates the linear parameter-varying component and the nonlinear uncertainty, providing a suitable structure for H∞ observer synthesis.

3.2. Observer Structure

The structural form of the observer is presented as follows:[17]

$$\begin{aligned} \dot{\hat{x}}(t) &= A(\rho(t))\hat{x}(t) + \\ &f_{\text{rem}}(\hat{x}(t)) + L(\rho(t))(y(t) - \hat{y}(t)); \\ \hat{y}(t) &= C\hat{x}(t) \end{aligned} \tag{15}$$

Define the estimation error as:

$$e(t) = x(t) - \hat{x}(t).$$

Substituting (13)–(15) yields the estimation error dynamics:

$$\dot{e}(t) = \big(A(\rho(t)) - L(\rho(t))C\big)e(t) + \Delta f(t) + B_w w(t) - L(\rho(t))D_v v(t) \quad (16)$$

where $\Delta f(t) = f_{\text{rem}}(x(t)) - f_{\text{rem}}(\hat{x}(t))$ and satisfies $\|\Delta f(t)\| \le L_f \|e(t)\|$. (17)

Equation (16) explicitly separates the effects of process disturbance $w(t)$ and measurement noise $v(t)$, which facilitates the subsequent H∞ analysis and LMI-based observer synthesis.

3.3. LMI Condition for $\mathcal{H}_\infty$ Observer

The following theorem provides sufficient conditions for exponential stability and H∞ performance of the proposed observer.

To ensure robustness against $w(t), v(t)$, and nonlinear uncertainties, a quadratic Lyapunov function $V(e) = e^\top P e$ is considered, with $P > 0$. The objective is to ensure: Exponential stability with decay rate $\beta > 0$, and $\mathcal{H}_\infty$ disturbance attenuation with level $\gamma > 0$. These requirements are enforced through the following dissipation inequality:

$$\dot{V}(e) + 2\beta P + e^\top e - \gamma^2 w^\top w - \gamma^2 v^\top v \le 0 \quad (18)$$

Calculate the derivative:

$$\dot{V}(e) = e^\top (A - LC)^\top P e + e^\top P (A - LC) e + 2e^\top P B_w w - 2e^\top P L D_v v + 2e^\top P \Delta f \quad (19)$$

Use Cauchy–Schwarz + Young[18,19]:

$$2e^\top P \Delta f \le 2 \| Pe \| \| \Delta f \| \le 2 \| P \| \| e \| \| \Delta f \| \quad (20)$$

For ease, use Young with the parameter $\epsilon_f > 0$:

$$2e^\top P \Delta f \le \epsilon_f \Delta f^\top \Delta f + \frac{1}{\epsilon_f} \quad (21)$$

Due $\| \Delta f \|^2 \le L_f^2 \| e \|^2$, we have:

$$\epsilon_f \Delta f^\top \Delta f \le \epsilon_f L_f^2 e^\top e. \quad (22)$$

If we choose ϵ_f and (or) normalize such that $\frac{1}{\epsilon_f} P^2 \le L_f^2 P$, then infer:

$$2e^\top P \Delta f \le L_f^2 e^\top P e. \quad (23)$$

Substitute (23) into 19:

$$\dot{V}(e) \le e^\top \big((A - LC)^\top P + P(A - LC) + L_f^2 P\big) e + 2e^\top P B_w w - 2e^\top P L D_v v \quad (24)$$

Introduce the standard change of variables:

$$L(\rho) = -P^{-1} Y(\rho) \quad (25)$$

which yields:

$$(A - LC)^\top P + P(A - LC) = A^\top P + PA + C^\top Y^\top + YC \quad (26)$$

At each grid vertex i, define:

$$\Xi_i = A_i P + P A_i^\top + C^\top Y_i^\top + Y_i C \quad (27)$$

Substituting (24), (26)–(27) into (18) gives

$$\dot{V} + 2\beta P + e^\top e - \gamma^2 w^\top w - \gamma^2 v^\top v \le e^\top \big(\Xi_i + 2\beta P + L_f^2 P\big) e + 2e^\top P B_{w,i} w + 2e^\top Y_i D_{v,i} v + e^\top e - \gamma^2 w^\top w - \gamma^2 v^\top v < 0$$

Rearranging terms yields the quadratic form:

$$\begin{bmatrix} e \\ w \\ v \end{bmatrix}^\top \begin{bmatrix} \Xi_i + 2\beta P + L_f^2 P & P B_{w,i} & Y_i D_{v,i} \\ B_{w,i}^\top P & -\gamma^2 I & 0 \\ D_{v,i}^\top Y^\top & 0 & -\gamma^2 I \end{bmatrix} \begin{bmatrix} e \\ w \\ v \end{bmatrix} < 0 \quad (28)$$

Inequality (28) is equivalent to the LMI condition

$$M = \begin{bmatrix} \Xi_i + 2\beta P + L_f^2 P & P B_{w,i} & Y_i D_{v,i} \\ B_{w,i}^\top P & -\gamma^2 I & 0 \\ D_{v,i}^\top Y^\top & 0 & -\gamma^2 I \end{bmatrix} < 0 \quad (29)$$

which must hold at each grid point $i = 1, \dots, N$.

Since the NLPV model is a convex interpolation of its vertices and a common Lyapunov matrix P is used, the feasibility of (19) at all vertices guarantees the dissipation inequality (18) for all admissible scheduling trajectories $\rho(t)$.

+ *Disturbance-free case* ($w = 0, v = 0$):

$\dot{V} + 2\beta V < 0 \Rightarrow \| e(t) \| \le c e^{-\beta t} \| e(0) \|$,

implying exponential stability with decay rate β.

+ *General case*: integrating (18) from 0 to ∞ yields:

$$\int_0^\infty \| e(t) \|^2 dt \le \gamma^2 \int_0^\infty (\| w(t) \|^2 + \| v(t) \|^2) dt,$$

establishing the desired $\mathcal{H}_\infty$ performance bound.

https://doi.org/10.52111/qnjs.2025.xxxxx

3.4. Gridding and Barycentric Interpolation Approach

To effectively design an observer for nonlinear parameter-varying systems, the state-dependent matrices $A(\rho(t))$ and $L(\rho(t))$ must be approximated. Direct continuous-time synthesis is generally intractable due to infinite-dimensional dependency on the scheduling parameter $\rho(t)$. Therefore, a gridding approach is adopted to discretize the state space.

The state space $X \subset x(t) \in \mathbb{R}^n$ is partitioned into a finite number of grid points $\{x^{[i]}\}_{1=1}^{N}$, where a local LMI observer synthesis is performed. At each grid point $x^{[i]}$, an observer gains $L^{[i]}$ is computed by solving the corresponding LMI condition. These gains are stored for online use.

To enable smooth gain variation and avoid chattering between discrete observers, the gains are interpolated during runtime using barycentric weights. Let $\hat{x}(t)$ denote the current observer state. The interpolated gain $L(\hat{x}(t))$ is calculated as:

$$L(\hat{x}(t)) = \sum_{i=1}^{N} \mu_i(\hat{x}(t))\, L^{[i]}, \tag{30}$$

where $\mu_i(\cdot)$ are barycentric interpolation weights satisfying $\sum_{i=1}^{N} \mu_i(\hat{x}(t)) = 1$, and $\mu_i \geq 0$.

4. NUMERICAL SIMULATION

This section evaluates the performance of the proposed gridding-based $\mathcal{H}_\infty$ NLPV observer on the Lorenz–63 system. The objective is to demonstrate robust state estimation under both process and measurement disturbances and to highlight the advantages of the proposed approach over conventional observers.

4.1. System Setup

The Lorenz 63 system is a well-known nonlinear chaotic system governed by the following differential equations:

$$\begin{aligned} \dot{x}(t) &= B_w w(t) + f(x(t)), \\ y(t) &= Cx(t) + D_w\, w(t) \end{aligned} \tag{31}$$

where $x(t) = [x_1,\ x_2, x_3]^{\top} \in \mathbb{R}^3$ is the system state, $w(t) \in \mathbb{R}^3$ denotes external disturbances, and the measurement output is $y(t) \in \mathbb{R}$. The matrices are defined as:

$$y(t) = Cx(t),\ C = [1 \quad 0 \quad 0]. \tag{32}$$

The nonlinear vector field $f(x)$ is given by[1]:

$$f(x(t)) = \begin{bmatrix} \sigma(x_2 - x_1) \\ x_1(\rho - x_3) - x_2 \\ x_1 x_2 - \beta x_3 \end{bmatrix} \tag{33}$$

with parameters $\sigma = 10, \rho = 28, \beta = \frac{8}{3}$. To facilitate observer design using convex optimization tools, we reformulate the nonlinear system into an NLPV structure by approximating the dynamics through local linearizations.

The nonlinear vector field $f(x)$ is linearized around multiple grid points $\{x^{(i)}\}_{i=1}^{N}$ within a bounded region $\mathcal{D} \subset \mathbb{R}^3$. At each point $x^{(i)}$, the Jacobian matrix is computed as:

$$A^{(i)} := J(x^{(i)}) = \frac{\partial f}{\partial x}\Big|_{x^{(i)}} \tag{34}$$

This results in a set of locally linearized models:

$$\dot{x}(t) \approx A^{(i)} x(t) + B_w w(t) + f_{\text{rem}}(x) \tag{35}$$

where $f_{\text{rem}}(x) := f(x) - A^{(i)} x$ is the residual nonlinearity. Assuming that $f(x)$ is Lipschitz continuous over $\mathcal{D}$, the residual satisfies:

$$\|f_{\text{rem}}(x) - f_{\text{rem}}(\hat{x})\| \leq L_f \|x - \hat{x}\|, \forall x, \hat{x} \in \mathcal{D} \tag{36}$$

for some constant $L_f > 0$. To express the system in NLPV form, we introduce a parameter trajectory $\rho(t) = \hat{x}(t)$, leading to:

$$\begin{aligned} \dot{x}(t) &= A(\rho(t))x(t) + B_w w(t) + f_{\text{rem}}(x) \\ y(t) &= Cx(t) + D_v v(t) \end{aligned} \tag{37}$$

The matrix $A(\rho(t))$ is obtained via online interpolation of $\{A^{(i)}\}$ using barycentric weights:

$$A(\rho(t)) = \sum_{i=1}^{N} \mu_i(\rho(t)) A^{(i)}, \tag{38}$$

$$\text{where } \sum_i \mu_i = 1, \mu_i \geq 0$$

This interpolation ensures a smooth and accurate approximation of the nonlinear dynamics across the grid.

https://doi.org/10.52111/qnjs.2025.xxxxx

Remark 2

The scheduling parameter is chosen as $\rho(t) = \hat{x}(t)$ to ensure real-time implementability of the observer. This avoids dependence on unmeasurable states while maintaining consistency between the NLPV model and the observer dynamics. As the estimation error converges, the scheduling variable naturally approaches the true state, thereby reducing interpolation mismatch.

4.2. Lipschitz Constant Estimation

The observer gains are designed at grid points uniformly sampled over $[-20, 20]^3$. At each grid point, the local Jacobian is computed and used to define $A(\rho_i)$.

The nonlinear drift term $f(x)$ of the Lorenz 63 system is defined in equation (27). To facilitate observer design with Lipschitz-type nonlinearities, the Lipschitz constant L_f is required. A vector field $f(x)$ is said to be Lipschitz continuous over the domain $\mathcal{D} \subset \mathbb{R}^n$ if there exists a scalar $L_f > 0$ which satisfies the equation (36).

A sufficient condition to obtain L_f is to evaluate the spectral norm of the Jacobian matrix $J(x)$:

$$L_f = \sup_{x \in \mathcal{D}} \|J(x)\|_2 \tag{39}$$

where $J(x) = \frac{\partial f(x)}{\partial x}$ is the Jacobian matrix of the drift function.

For the Lorenz system, the Jacobian is computed as:

$$J(x) = \nabla f(x) = \begin{bmatrix} -\sigma & \sigma & 0 \\ \rho - x_3 & -1 & -x_1 \\ x_2 & x_1 & -\beta \end{bmatrix} \tag{40}$$

The spectral norm $\|J(x)\|_2$ is the largest singular value of $J(x)$, which can be numerically evaluated over a bounded region $\mathcal{D}$. In this work, the domain is chosen as $\mathcal{D} = [-20, 20]^3$, covering the typical range of Lorenz state trajectories.

A grid-based scan of $J(x)$ across $\mathcal{D}$ yields an upper bound: $L_f \approx 56.6092$

Figure 1 describes the distribution of $\|J(x)\|_2$ over a bounded domain in (x_1, x_2, x_3). It is observed that the spectral norm varies significantly, reaching values above $L_f = 56.6092$ in lower regions of the state space (i.e., $x_3 < 0$), while staying below 25 in upper regions (i.e., $x_3 > 10$). This spatial variability reflects the strong local nonlinearity of the Lorenz system, which motivates the use of a gridding-based observer design. By selecting local Lipschitz bounds within each grid cell, the observer gain can be adapted more accurately to the system's local dynamics, avoiding conservatism associated with a global Lipschitz constant.

This bound is used in the LMI formulation to handle the nonlinear remainder term using Lipschitz inequalities, ensuring robust estimation even in the presence of nonlinear uncertainties.

Using CVX toolbox and semidefinite programming (SDP)[20], a set of LMI conditions is solved to obtain observer gains $\{L_i\}$. At runtime, the gain $L(\hat{x})$ is interpolated using barycentric weights based on proximity to the grid centers.

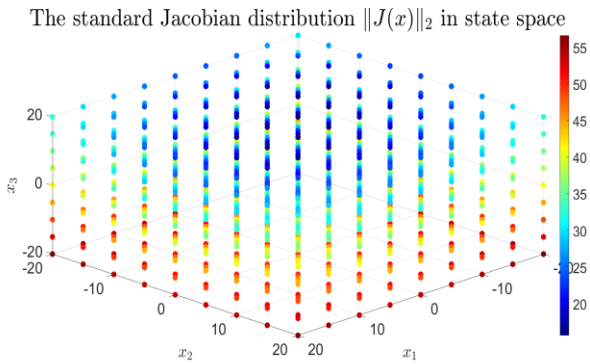

Figure 1. A graph representation of the Jacobian $\|J(x)\|_2$ in the state space.

Specifically, for each grid point $i \in \{1, 2, \ldots, 4\}$ of the NLPV system in equation (24), the LMI condition in equation (29) is solved to synthesize a robust $\mathcal{H}_\infty$ observer.

The CVX toolbox in MATLAB is employed to solve the optimization problem and compute the observer gain matrices L_i corresponding to each value of the scheduling parameter ρ, using the system matrices defined in section 3.4.

https://doi.org/10.52111/qnjs.2025.xxxxx

The optimization yields a disturbance attenuation level of $\gamma = 0.0023$. The resulting observer gain $L(\hat{x})$ of the four grid points of ρ are as follows:

$$L(\hat{x}) = [519.9294; -17.1069; 6.3601]^T$$

4.3. Simulation Scenarios and Discussion

To evaluate and compare the performance of the proposed $\mathcal{H}_\infty$ observer and the EKF[9], numerical simulations are carried out on the Lorenz 63 system. The initial state of the system is set as $x(0) = [-5, -5, -5]^T$, and both observers are initialized at the origin $[0, 0, 0]^T$. The EKF is implemented using a first-order prediction-correction structure, where the time-varying Jacobian matrix of the Lorenz system is used in the prediction step. The initial covariance matrix is selected as $P_0 = 2 \cdot I_3$ to ensure sufficient initial uncertainty for the EKF. In contrast, the $\mathcal{H}_\infty$ observer uses a gridding structure interpolated via barycentric weights over a predefined grid of the state space.

To provide a comprehensive performance analysis, two sets of simulation conditions are examined:

Noise-Free Scenario: The system evolves without any disturbances to establish a baseline.

Figure 2 illustrates the comparison between the actual states x_1 to x_3 and their corresponding estimated values $\hat{x}_1$ to $\hat{x}_3$. In the plots, the solid green line represents the true system states, the red dashed line indicates the estimates from the proposed $\mathcal{H}_\infty$ observer, while the blue dash-dot line corresponds to the estimates obtained using the EKF.

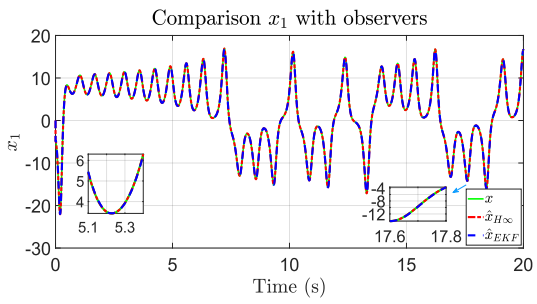

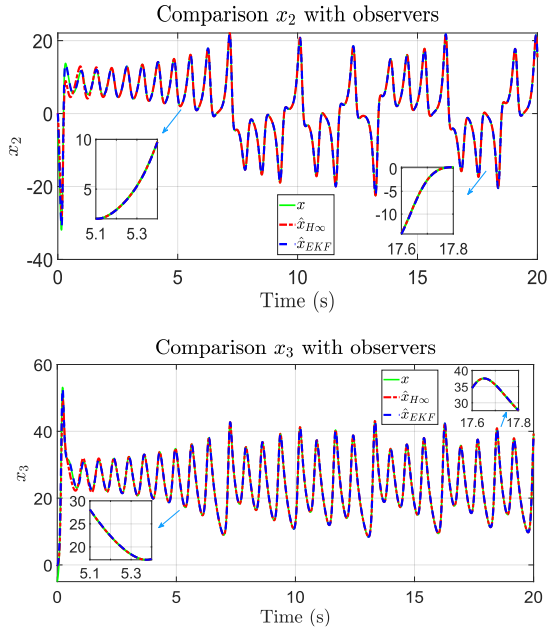

Figure 2. Comparison of system states with noise-free

It is evident from Figure 2 plots that both $\mathcal{H}_\infty$ observer and the EKF closely track the true system states. The estimation errors are negligible for all state variables, reflecting excellent accuracy in the absence of noise. Notably:

In x_1, both observers almost overlap with the ground truth across the entire time span, with only very slight divergence in highly dynamic segments. The inset zoomed plots confirm sub-millisecond response agreement.

In x_2, the estimations remain aligned even during sharp transient oscillations. This highlights the observers' ability to capture rapid nonlinear dynamics.

In x_3, where chaotic oscillations dominate, both $\hat{x}_{\mathcal{H}_\infty}$ and $\hat{x}_{EKF}$ accurately replicate the system evolution.

In the noise-free scenario, both the proposed gridding-based NLPV $\mathcal{H}_\infty$ observer and the EKF provide accurate state estimation, indicating that both approaches are capable of tracking the Lorenz dynamics under ideal measurement conditions.

Nevertheless, a closer inspection of the zoomed-in sub-figures reveals subtle but consistent differences between the two observers. In particular, the proposed observer exhibits a slightly reduced phase lag during transient convergence, as

https://doi.org/10.52111/qnjs.2025.xxxxx

well as smoother tracking behavior with fewer oscillatory artifacts. These differences become more visible in time intervals characterized by rapid state variations, where local linearization effects may limit the EKF performance.

Although the overall estimation accuracy of both observers is comparable in this noise-free case, the observed improvements indicate that the proposed gridding-based NLPV formulation provides a more consistent representation of the underlying nonlinear dynamics, even in the absence of disturbances.

Noisy Scenario: Both process and measurement noise are activated.

The state dynamics are subjected to an additive zero-mean Gaussian process noise $w(t) \sim \mathcal{N}(0, Q)$ and measurement noise $v(t) \sim \mathcal{N}(0, R)$, where the covariance matrices are chosen as follows:

$$Q = 0.5 \cdot I_3, R = I_1 \tag{41}$$

The process noise $w(t)$ is generated at each time step as:

$$w_k = \sqrt{Q} \cdot \omega_k, \omega_k \sim \mathcal{N}(0, I_3) \tag{42}$$

while the measurement noise is:

$$v_k = \sqrt{R} \cdot v_k, v_k \sim \mathcal{N}(0, I_1) \tag{43}$$

Figure 3 compares the actual states x_1 to x_3 and their corresponding estimated values $\hat{x}_1$ to $\hat{x}_3$, in the presence of noise as described above. The figures demonstrate that both observers track the system well, but the performance diverges during fast transients and in regions of strong nonlinear coupling.

Estimation of x_1: During the early transient phase around $t \in [5.1, 5.3]$s (left zoom-in), the trajectories of the true state and both observers start to converge after a rapid change in system dynamics. The zoomed view clearly shows that the proposed $\mathcal{H}_\infty$ observer tracks the true state with smaller phase lag and reduced oscillation amplitude compared to the EKF. This behavior indicates a faster convergence rate, which is consistent with the explicit decay-rate constraint incorporated in the LMI-based observer design.

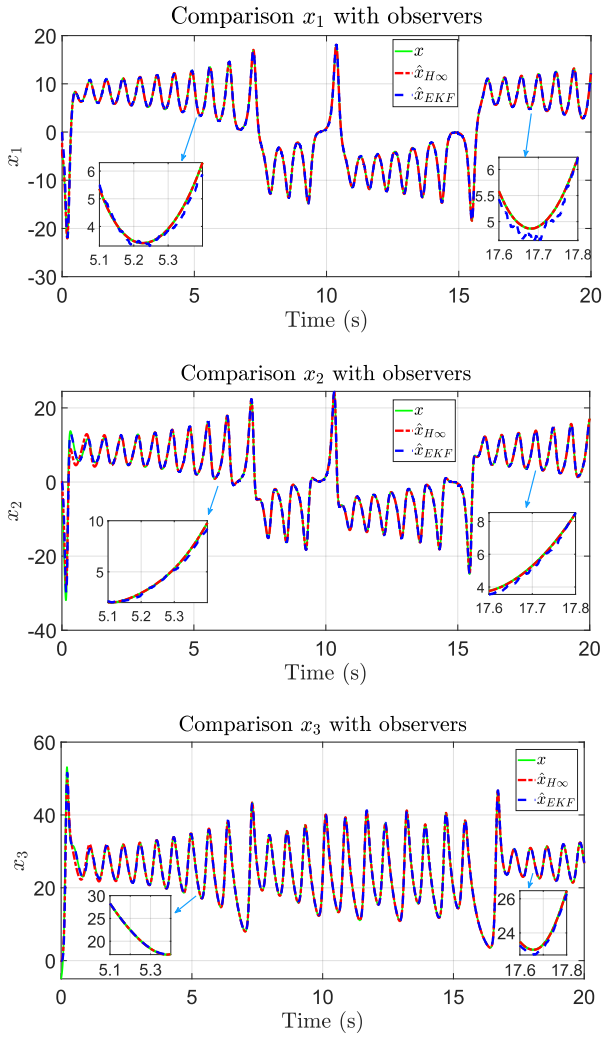

Figure 3. Comparison of system states with noise

In the highly nonlinear region around $t \in [17.6, 17.8]$s (right zoom-in), the Lorenz system exhibits sharp peaks and rapid variations. In this interval, the EKF estimation shows noticeable deviations from the true state, whereas the proposed $\mathcal{H}_\infty$ observer maintains closer alignment. This demonstrates the improved robustness of the proposed approach against nonlinear amplification effects and disturbances in regions where local linearization becomes less accurate.

For the second state x_2, the zoomed-in interval $t \in [5.1, 5.3]$s highlights the convergence behavior during a steep state transition. The proposed observer exhibits a smoother transient response with reduced overshoot compared to the EKF. This

https://doi.org/10.52111/qnjs.2025.xxxxx

suggests that the proposed method effectively balances convergence speed and robustness, avoiding aggressive corrections that can amplify noise.

In the later interval $t \in [17.6, 17.8]$s, where x_2 undergoes rapid sign changes and strong nonlinear coupling, the EKF trajectory deviates more significantly from the true state. In contrast, the proposed $\mathcal{H}_\infty$ observer remains tightly bounded around the true trajectory. This confirms the advantage of the gridding-based NLPV formulation, which captures dominant variations of the Jacobian over the attractor domain and provides robustness beyond local linearization.

Estimation of x_3: The estimation results for x_3 further emphasize the robustness properties of the proposed observer. In the zoomed-in window around $t \in [5.1, 5.3]$s, both observers converge toward the true state; however, the proposed $\mathcal{H}_\infty$ observer shows smaller steady-state oscillations once convergence is achieved.

More importantly, in the interval $t \in [17.6, 17.8]$s, where x_3 reaches higher amplitudes and the effect of nonlinear coupling is pronounced, the EKF exhibits increased estimation error. The proposed observer, on the other hand, maintains accurate tracking with reduced sensitivity to noise. This behavior highlights the effectiveness of explicitly accounting for nonlinear remainder bounds and disturbance attenuation in the observer design.

Tables 1–3 present the state estimation performance indices, including RMSE, NRMSE, and the R^2- for both the EKF and the proposed $\mathcal{H}_\infty$ observer, under noise-free and noisy conditions, respectively.

- Root Mean Square Error (RMSE):

$$\text{RMSE}_i = \sqrt{\frac{1}{N}\sum_{k=1}^{N} (x_i(k) - \hat{x}_i(k))^2} \qquad (38)$$

- Normalized RMSE (NRMSE):

$$\text{NRMSE}_i = \frac{\text{RMSE}_i}{\max(x_i) - \min(x_i)} \qquad (39)$$

- Coefficient of Determination (R^2) :

$$R_i^2 = 1 - \frac{\sum (x_i - \hat{x}_i)^2}{\sum (x_i - \bar{x}_i)^2} \qquad (40)$$

Table 1. RMSE index of states

RMSE	With noise-free		With Noise	
	EKF	$\mathcal{H}_\infty$	EKF	$\mathcal{H}_\infty$
x_1	0.04042	0.00197	0.25921	0.00313
x_2	0.06177	0.15654	0.33442	0.16664
x_3	0.07490	0.16884	0.27328	0.17989

Table 2. NRMSE index of states

N RMSE	With noise-free		With Noise	
	EKF	$\mathcal{H}_\infty$	EKF	$\mathcal{H}_\infty$
x_1	0.00114	5.62e-05	0.00757	9.14e-05
x_2	0.00131	0.00336	0.00743	0.00370
x_3	0.00197	0.00455	0.00679	0.00447

Table 3. R^2 index of states

R^2	With noise-free		With Noise	
	EKF	$\mathcal{H}_\infty$	EKF	$\mathcal{H}_\infty$
x_1	0.99996	1.00000	0.99896	0.99999
x_2	0.99995	0.99968	0.99857	0.99964
x_3	0.99991	0.99955	0.99872	0.99944

The numerical values reported in Tables 1–3 are computed directly from the full simulated state trajectories over the specified time intervals, whereas Figures 2 and 3 provide qualitative visualization of the corresponding estimation performance.

The simulation results demonstrate a comprehensive comparison between the proposed $\mathcal{H}_\infty$ observer and the EKF under both noise-free and noisy conditions. As presented in Tables 1–3, the $\mathcal{H}_\infty$. The observer exhibits superior robustness, especially in the presence of process and measurement noise.

In the noise-free scenario, EKF achieves slightly better RMSE values for x_2 and x_3, while the $\mathcal{H}_\infty$ observer delivers the best accuracy for x_1, achieving an RMSE of only 0.00197 and a coefficient of determination $R^2 =$ 1.0000. However, in the noisy case, the performance of EKF significantly degrades across all states. For

https://doi.org/10.52111/qnjs.2025.xxxxx

instance, the RMSE for x_1 increases to 0.25921 under EKF, whereas the proposed observer maintains a remarkably low RMSE of 0.00313.

The NRMSE analysis further supports these findings, with the $\mathcal{H}_\infty$ observer consistently achieves lower normalized errors under noisy conditions. Specifically, for x_1, the NRMSE of the $\mathcal{H}_\infty$ observer remains as low as 9.14×10^{-5}, compared to 7.57×10^{-3} for EKF.

In terms of the coefficient of determination, the $\mathcal{H}_\infty$ observer consistently attains higher R^2 values in both scenarios, indicating a better match between estimated and actual states. Notably, the observer preserves an R^2 of over 0.9999 for all states even in the presence of noise, whereas EKF drops to 0.9985 or lower.

Overall, these results validate the robustness and estimation accuracy of the proposed $\mathcal{H}_\infty$ observer design. The gridding-based LMI synthesis, combined with barycentric interpolation of the observer gain, enables the observer to maintain high precision under strong nonlinearities and measurement uncertainties. In contrast, EKF performance is more sensitive to noise and model mismatch, highlighting the conservative yet effective design philosophy of the $\mathcal{H}_\infty$ approach.

5. CONCLUSIONS

This paper has developed a gridding-based NLPV $\mathcal{H}_\infty$ observer for the Lorenz–63 system, addressing the challenges posed by strong nonlinear coupling and chaotic dynamics. By reformulating the original nonlinear system into an NLPV structure with an explicitly bounded nonlinear remainder, the proposed approach enables a convex LMI-based observer synthesis with guaranteed stability properties.

The main results demonstrate that the proposed observer ensures exponential convergence of the estimation error with a prescribed decay rate and achieves effective attenuation of both process disturbances and measurement noise. The use of a small number of representative grid points allows a practical trade-off between robustness and computational efficiency while maintaining feasibility of a common Lyapunov function.

Simulation results confirm that, in the noise-free case, the proposed observer provides comparable accuracy under ideal conditions and improved robustness in the presence of disturbances compared to the EKF. Under disturbed conditions, the proposed method exhibits superior robustness, with reduced sensitivity to noise and improved estimation accuracy across all state variables.

Overall, the results validate the effectiveness of the proposed gridding-based NLPV $\mathcal{H}_\infty$ observer as a reliable and robust estimation framework for nonlinear chaotic systems. Future work will investigate extensions to higher-dimensional nonlinear systems and experimental validation on physical platforms.

REFERENCES

1. E. N. Lorenz. Deterministic Nonperiodic Flow," *J. Atmos. Sci.*, **1963**, *20*(2), 130–141.
2. M. Goodliff, S. Fletcher, A. Kliewer, J. Forsythe, A. Jones. Detection of non-Gaussian behavior using machine learning techniques: a case study on the Lorenz 63 model, *Journal of Geophysical Research: Atmospheres*, **2020**, 125(2), e2019JD031551.
3. P. Tandeo, P. Ailliot, J. Ruiz, A. Hannart, B. Chapron, A. Cuzol, and R. Fablet. Combining analog method and ensemble data assimilation: application to the Lorenz-63 chaotic system, *Proceedings of the 4th International Workshop on Climate Informatics , Springer International Publishing,* **2015**, 3-12.
4. F. Zhu, Y. Fu, T. N. Dinh. Asymptotic convergence unknown input observer design via interval observer, *Automatica,* **2023**, *147*, 110744. 10.1016/j.automatica.2022.110744
5. C. M. Nguyen, A-T. Nguyen, S. Delprat. Cascade Takagi-Sugeno Fuzzy Observer Design for Nonlinear Uncertain Systems with Unknown Inputs: A Sliding Mode Approach, *International Journal of Robust and Nonlinear Control*, **2023**, *33*(15) 9066-9083 DOI: 10.1002/rnc.6371
6. T-P. Pham, O. Sename, L. Dugard. A nonlinear parameter varying observer for real-time damper force estimation of an automotive electro-rheological suspension system, *International*

Journal of Robust and Nonlinear Control, **2021**, *31*(17),8183-8205.https://doi.org/10.1002/rnc.5583

7. S. Meng, F. Meng, F. Zhang, Q. Li, Y. Zhang, A. Zemouche. Observer design method for nonlinear generalized systems with nonlinear algebraic constraints with applications, *Automatica*, **2024**, *162*, 111512. 10.1016/j.automatica.2024.111512
8. S. Mohite, M. Alma, A. Zemouche. Toward enhancing nonlinear observers for Lipschitz system: Exploiting the matrix multipliers-based LMIs, *International Journal of Robust and Nonlinear Control*, **2024,** *34*(15), 10799-10820. https://doi.org/10.1002/rnc.7552
9. C. O. Ongere, D. Angwenyi, R. Oryiema. Second order Extended Ensemble Kalman Filter with Stochastically Perturbed Innovation, *Science Mundi,* **2024**, *4*(2), 222-242
10. Hazazi, Muhammad Asaduddin and Sihabuddin. Extended Kalman filter in recurrent neural network: USDIDR forecasting case study, *Indonesian Journal of Computing and Cybernetics Systems*, **2019,** *13*(3), 293. DOI:10.22146/ijccs.47802
11. S. Mohite, M. Alma, A. Zemouche, M. Haddad. LMI-based H∞ observer design for nonlinear Lipschitz system, *IFAC-PapersOnLine,* **2023**, *56* (2), 6745-6750.10.1016/j.ifacol.2023.10.380
12. E. Chnib, P. Bagnerini, A. Zemouche. LMI based H∞ Observer Design for a Quadcopter Model Operating in an Adaptive Vertical Farm, *IFAC-PapersOnLine*, **2023,** *56*(2), 10837-10842. https://doi.org/10.1016/j.ifacol.2023.10.757
13. K-T. Vo, T. D. Le, T-P. Pham. Design of an H∞ observer for nonlinear parameter-varying systems with lipschitz nonlinearity and model uncertainty, *UD-JST,* **2025,** *vol 23 (9B),* 34–39, https:doi.org/10.31130/ud-jst.2025.23(9B).501E
14. J-P. Berrut, L. N. Trefethen. Barycentric Lagrange Interpolation, *Society for Industrial and Applied Mathematics*, **2004**, *46*(3), 501–517. DOI. 10.1137/S0036144502417715
15. A. H. Jazwinski. *Stochastic Processes and Filtering Theory*, **1970,** iii-ix, 1-376
16. K. Ito. 109. Stochastic Integral, *Proceedings of the Imperial Academy*, **1944**, *20*(8), 519-524
17. D. G. Luenberger. Observing the state of a linear system", *IEEE Transactions on military electronics*, **1964**, *8* (2), 74-80.
18. H. K. Khalil, *Nonlinear Systems*, 3rd Ed., Prentice Hall, **2002**.
19. S. Boyd and L. El Ghaoui et al., *Linear Matrix Inequalities in System and Control Theory*, SIAM, **1994**.
20. M. Grant, and S. Boyd (**2014**). CVX: Matlab software for disciplined convex programming, version 2.1. http://cvxr.com/cvx.